Partitioning the sediment flux by provenance and tracing erosion patterns in Taiwan

Alberto Resentini[1], Liran Goren[2], Sebastien Castelltort[3], Eduardo Garzanti[1]

[1] Laboratory for Provenance Studies, Department of Earth and Environmental Sciences, University of Milano-Bicocca, 20126 Milano, Italy

[2] Department of Geological and Environmental Sciences, Ben Gurion University of the Negev, 84105 Beer-Sheva, Israel

[3] Department of Earth Sciences, University of Geneva, 1205 Geneva, Switzerland

Corresponding author: Alberto Resentini (alberto.resentini@unimib.it)

Key Points:

- Quantitative provenance analysis of modern sand allows refined resolution in tracing erosion rates
- Provenance and morphometric data show focused erosion in the retro-side of the Taiwan orogen

ABSTRACT

We illustrate and critically evaluate the potential and limitations of a refined alternative way to calculate erosion rates, based on petrographic and mineralogical fingerprints of fluvial sediments coupled with gauged sediment fluxes. Our approach allows us to reapportion sediment loads to different lithological units in each catchment, and consequently to discriminate erosion rates in different tectonic domains with enhanced spatial resolution. Provenance data on modern Taiwan sands imply focused erosion in the Backbone Range and Tananao Complex of the retro-wedge. Lower rates characterize the northern part of the island characterized by tectonic extension and the western foothills in the pro-wedge. The principal factor of uncertainty affecting our estimates is the inevitably inaccurate evaluation of total sediment load. Another is the assumption that suspended load and bedload are derived from the same sources in the same proportions. Additional errors are caused by the insufficiently precise definition of lithologically-similar compositional end-members, and by the temporal variability of sediment composition at the outlet of each catchment related to the spatial variability of erosional processes and triggering agents such as earthquakes, typhoons and landslides. To critically evaluate the robustness of our estimates we applied a morphometric technique based on the stream-power model. The results obtained with the two techniques are broadly consistent, with local discrepancies ascribed to poorly constrained assumptions and choices of scaling parameters. Our estimates are consistent with GPS uplift rates measured on a decadal timescale, and generally higher than those inferred from cosmogenic-nuclide and thermochronology data reflecting longer timescales.

> "*For what are we to do on the Last Day, when the works of human kind are weighed, with three treatises on formic acid, or even thirty? On the other hand, what do we know about the Last Day, if we don't even know what may have become of formic acid by then?*"
> Robert Musil, The man without qualities, vol. 1, p.268.

1. INTRODUCTION

Taiwan is one of the world's foremost natural laboratories for studies of orogenesis (Figure 1). After only a few Ma of ongoing collision between the Chinese continental margin and the Luzon Arc, the associated orogen has reached already nearly 4 km in height and 100-150 km in width. High rates of convergence leading to rapid rock uplift combine with the wet stormy climate of the sub-tropical typhoon belt to deliver annually an average detrital mass of 9500 t/km^2 [*Kao and Milliman*, 2008]. The doubly-vergent thrust belt is composed for more than 85% of sedimentary rocks dominant in the pro-wedge, but metamorphic rocks as young as < 10 Ma are exposed in the retro-wedge, where zircon fission-track, apatite fission-track and (U-Th)/He ages are all reset and as young as 1 Ma or younger, indicating very recent fast exhumation [*Jahn et al., 1986*; *Simoes et al., 2012*]. There is hardly another region where rock-uplift, unroofing and sediment production are of equal intensity.

Quantitative analyses of tectonic and erosional processes around Taiwan have been carried out following diverse independent ways, including estimates of fluvial discharge of suspended solids [*Li, 1976*; *Hwang, 1982*; *Fuller et al., 2003*; *Dadson et al., 2003*], thermochronological techniques [*Willett et al., 2003*; *Fuller et al., 2006*], cosmogenic measurements [*Schaller et al., 2005*; *Siame et al., 2011*; *Derrieux et al., 2014*], leveling and GPS surveys [*Liu and Yu, 1990; Ching et al., 2011*], and morphometry of river profiles [*Fox et al., 2014*]. Also the appearance and relative abundance of diagnostic rock fragments and other detrital minerals in Plio-Pleistocene sedimentary successions has been used to constrain patterns and rates of unroofing [*Lee, 1977*; *Dorsey, 1988*], but a systematic description of compositional signatures of sediments shed by distinct tectonic domains has not been carried out so far.

In this article we combine petrographic and heavy-mineral analyses of modern sands carried by rivers all around Taiwan with their available sediment loads to calculate the detrital volumes generated from different lithological assemblages within the orogen. River sediments are powerful integrators of information that efficiently mediate provenance signals from different parts of the entire watershed [D. Burbank in *Greensfelder, 2002*], thus offering a great advantage relative to other techniques focused on bedrock. Provenance-derived erosion rates are finally compared with geomorphological analyses based on the stream power model [*Whipple and Tucker, 1999*] in order to investigate the spatial and temporal resolution of the two techniques.

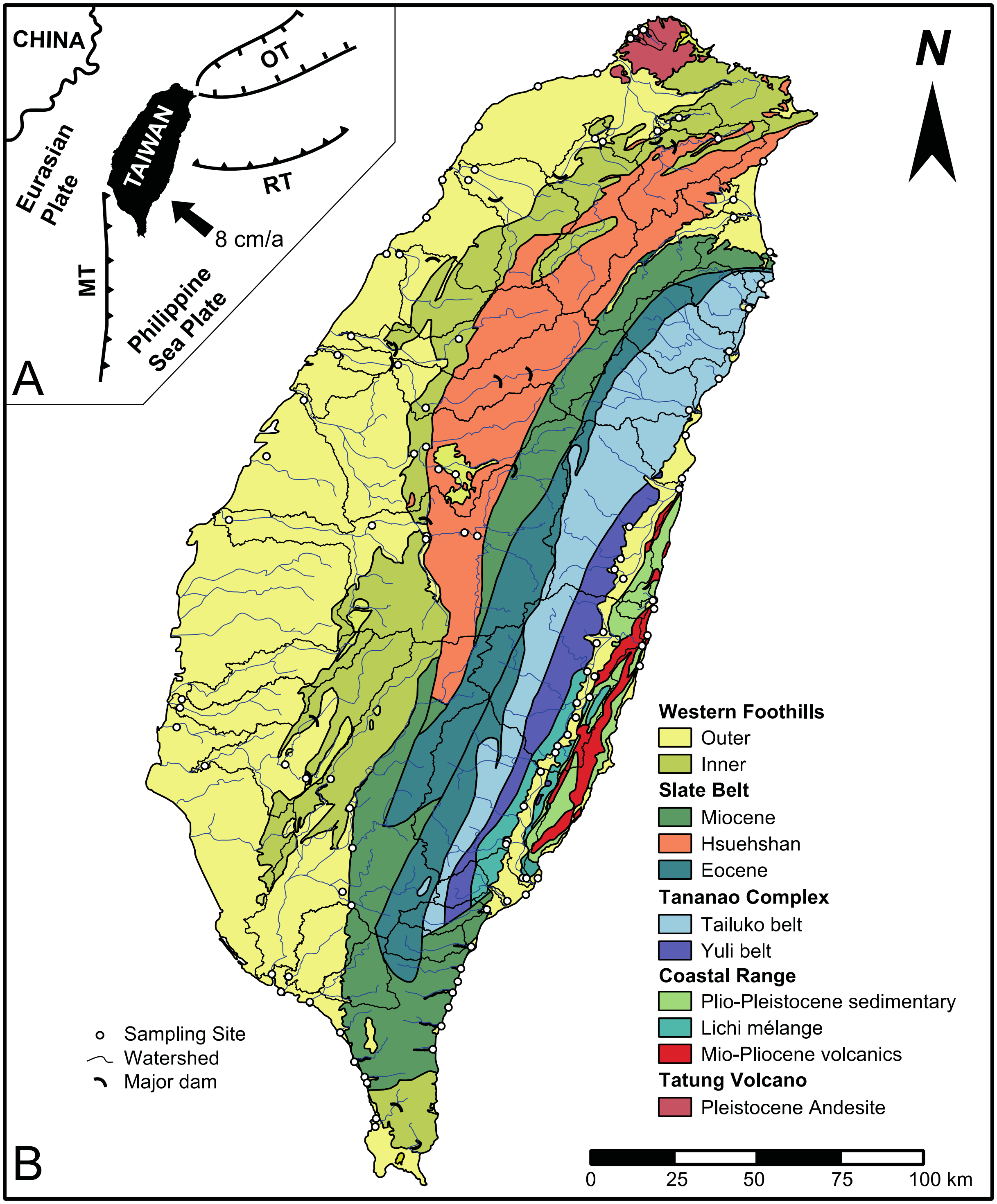

Figure 1: A) Geodynamic setting of Taiwan (after *Dadson et al., 2004*): MT, Manila Trench; OT, Okinawa Trough; RT, Ryukyu Trench; B) Geology of Taiwan (after *Central Geological Survey, 2000*). Major river basins and sampling sites are indicated.

2. GEOLOGY, GEOMORPHOLOGY AND SEDIMENT FLUX

The Taiwan orogen, formed during eastward subduction of the Chinese passive continental margin beneath the Luzon Arc on the Philippine Sea Plate, has long been considered as an archetypal product of arc-continent collision [*Ho, 1986*; *Byrne et al., 2011*]. Marked obliquity of colliding margins resulted in a "zipper effect", with closure of the South China Sea and collision onset becoming progressively younger southwards. At the same time, in northern Taiwan the orogen is being disrupted by normal faults associated with south-westward propagation and roll-back of the Ryukyu subduction zone and consequent intra-arc rifting and back-arc spreading in the Okinawa Trough [*Suppe, 1984*; *Teng, 1996*; *Shinjo et al., 1999*]. This ongoing process is responsible for andesitic volcanism in the northern Taiwan volcanic zone (e.g. Tatun volcano group, *Song et al., 2000*; *Wang et al., 2004*; *Shellnut et al., 2014*).

The boundary between the Eurasian and Philippine Sea plates runs along the Longitudinal Valley. The Coastal Range in the east represents the northern extension of the Luzon Arc, and includes Neogene volcanic rocks and Plio-Pleistocene siliciclastic deposits (Figure 1; *Chang and Chi, 1983*; *Huang et al., 2006*). The Central Range includes polymetamorphic basements rocks (Tananao Complex) and a Slate Belt (Backbone Range and Hsuehshan Range), representing the Chinese continental margin hyper-extended during latest Cretaceous-Paleocene rifting and its Cenozoic sedimentary cover [*Teng et al., 1991*; *Malavieille et al., 2002*; *McIntosh et al., 2013*]. The Western Foothills incorporate Oligo-Miocene sediments of the Chinese passive margin and younger foreland-basin deposits accreted along the frontal part of the orogen [*Mouthereau et al., 2002*; *Lin et al., 2003*; *Nagel et al., 2014*].

2.1. Climate and sediment fluxes

The island of Taiwan (~36,000 km^2), lying at tropical latitudes between N°21'54 and N°25'18, has mild climate throughout the year, with average annual temperatures ranging from 22°C in the north to 24°C in the south. Frost or snow may occur on the high mountains in winter, whereas temperatures may reach 38°C in summer. The island has 286 peaks above 3,000 m a.s.l., reaching 3,952 m on the summit of Jade mountain. Annual rainfall, between 65% and 90% of which concentrated between May and October, is on average 2.0-2.5 m along the eastern coast, reaches 3 m in the central range and in the north, and decreases to 1.5 m or less along the western coast; the northern foothills and mountain areas may receive up to 5 m or even 6 m of rain annually (Figure 2). Typhoons, hitting the island from the Pacific Ocean four to five times per year on average and mostly between July and September, may bring more than 2 m of torrential rain in 48 hours, triggering multiple massive mudslides and rockslides [*Hovius et al., 2000*; *Dadson et al., 2005*;

Montgomery et al., 2014]. Extreme sediment yields from the Taiwan orogen result from such harsh climatic conditions coupled with rapid tectonic deformation, extreme relief, and frequency of high-magnitude earthquakes [*Dadson et al., 2004*; *Shyu et al., 2005*].

The largest rivers draining ≥ 1000 km^2 are the Tanshui in northern Taiwan, the Dajia, Dadu, Zhuoshui, Kaoping and Tsengwen in western Taiwan, and the Lanyang, Hualian, Xiuguluan and Beinan in eastern Taiwan. The main characteristics of drainage basins, including water and sediment fluxes, sediment yields and estimated erosion rates are provided in Supplementary Table A1. Bathymetric surveys of water reservoirs between 1970 and 1998 and their correlation with suspended-load estimates in corresponding catchments allowed Dadson et al. [2003] to assess with 95% confidence that total river load in mountain areas is composed of 70±28% suspended load and 30±28% bedload.

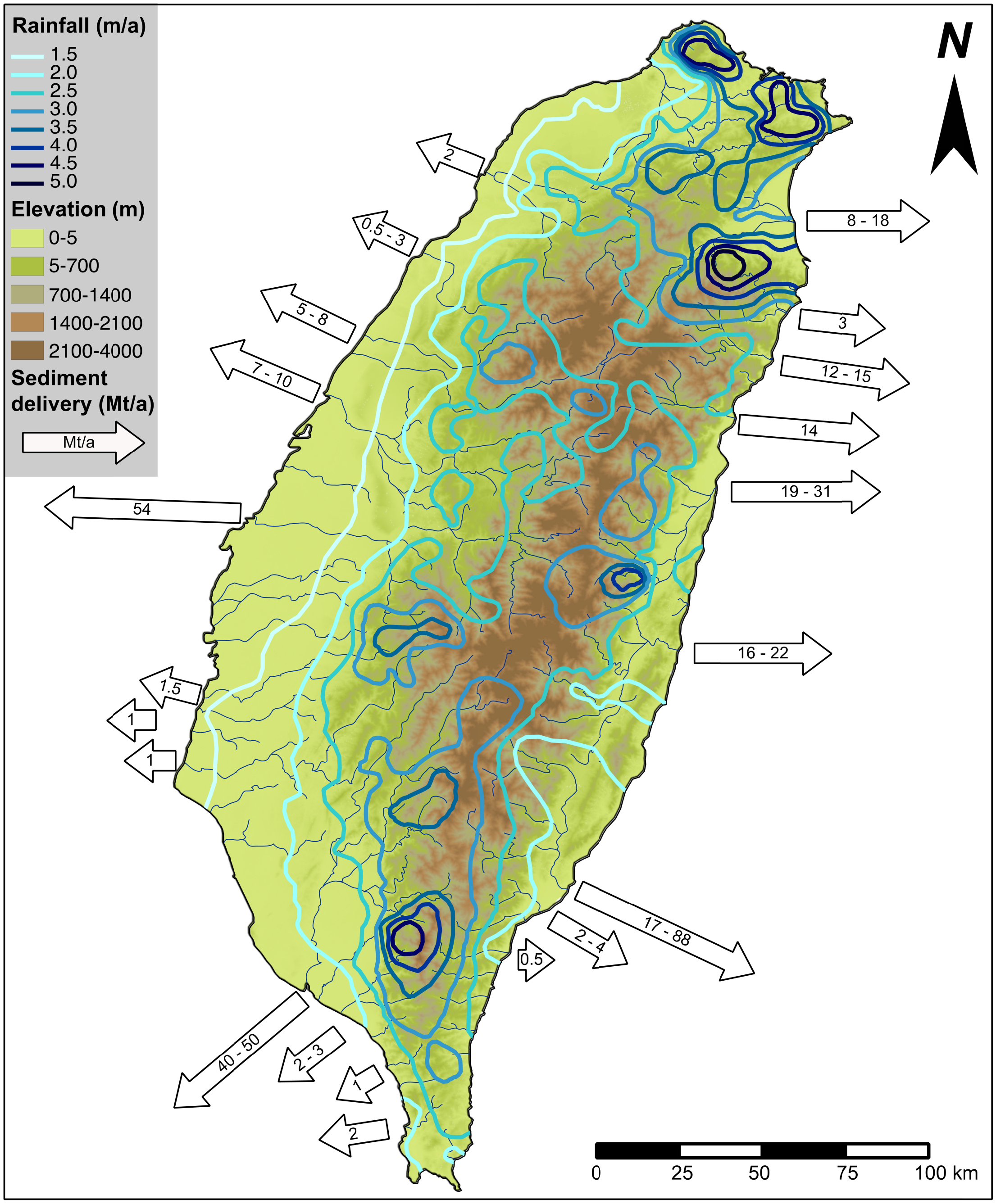

Figure 2: Elevation, annual rainfall and sediment delivery. Elevation data after SRTM v.4 [*Jarvis et al., 2008*], rainfall data (1949-2009) from Taiwan Water Resources Agency. Mean annual sediment fluxes from Hwang [1982], Dadson et al. [2003] and Liu et al. [2008].

2.2. Uplift and erosion rates

Uplift and erosion rates in the Taiwan orogen have long been assessed with various independent methods to range between 3 and 7 mm/a on average, and to reach up to 60 mm/a locally (Table A1; *Dadson et al., 2004*). Earlier estimates of uplift and denudation were based on suspended river load and sediment production during the Plio-Pleistocene [*Li, 1976*], progressive exhumation of the Slate Belt as documented by sandstone petrography [*Lee, 1977*], fault displacements and elevation changes [*Bonilla, 1977*], radiocarbon dates of raised Holocene coral reefs [*Peng et al., 1977*], and fission-track ages of zircon, apatite, and sphene from granitoid gneisses of the Tailuko Belt [*Liu, 1982*]. Dorsey [1988] combined the unroofing history recorded by petrographic trends through the Plio-Pleistocene terrigenous succession of the Coastal Range with pressure-temperature-time paths of Tananao metamorphic rocks to infer uplift rates of 4-5 mm/a. Lundberg and Dorsey [1990] calculated minimum rates of 5.9 to 7.5 mm/a by measuring the total uplift of Coastal Range marine strata in the last Ma. Dadson et al. [2003] estimated erosion rates of 3-6 mm/a from modern river suspended loads, Holocene river incision and apatite fission-track data. From suspended sediment loads, Fuller et al. [2003] estimated erosion rates varying along the retro-wedge between 2.2 mm/a (Hualien catchment) and 8.3 mm/a (Xiuguluan catchment). Fuller et al. [2006] used zircon and apatite fission-track data to infer maximum average erosion rates of ~3.3 mm/a for the retro-wedge and ~2.3 mm/a for the entire island, with highest rates of 6-8 mm/a on the steep flanks of the mountain belt and lowest rates < 2 mm/a in the foreland basin to the west, revising the higher estimates of 4-6 mm/a obtained previously [*Willett et al., 2003*]. Based on concentration of cosmogenic ^{36}Cl, an average rate of fluvial incision as high as 26±3 mm/a was calculated to have taken place throughout the middle and late Holocene in the gorge of the Liwu River cutting across the metamorphic Tailuko Belt [*Schaller et al., 2005*]. Raman spectroscopy of carbonaceous material, fission-track and (U-Th)/He ages of detrital zircons, allowed Simoes et al. [2007] to estimate uplift rates of 4.2 mm/a for the Hsuehshan Range and 6.3 mm/a for the Tananao metamorphic complex. Siame et al. [2011] assessed erosion rates in the Lanyang catchment to be 2±1 mm/a based on the concentration of cosmogenic ^{10}Be in detrital quartz and 4.6 mm/a based on suspended-load data. Also based on the concentration of cosmogenic ^{10}Be in detrital quartz, Derrieux et al. [2014] determined denudation values of 4-5 mm/a slightly increasing southward for the retro-wedge, and of 1-3 mm/a for the pro-wedge with a minimum value obtained for the Dadu catchment in central Taiwan. From the study of river profiles, Fox et al. [2014] inferred that current rock-uplift rates exceed erosion rates across much of the island, with an increase in uplift rates in the axial part of the orogen during the last 500 kyr.

3. PETROGRAPHIC AND HEAVY-MINERAL SIGNATURES

To quantify sediment supply from different rivers all around the island of Taiwan, and to characterize at best the end-member petrographic and mineralogical fingerprints of detritus produced in all tectonic domains and shed by different source-rock lithologies, in October 2012 we collected 85, mostly fine- to medium-grained sand samples from active bars of 73 different rivers, including all major ones as well as smaller streams draining specific geological units only.

Sands were impregnated with Araldite, cut into standard thin sections stained with alizarine red to distinguish dolomite and calcite, and analyzed by counting 400 points under the microscope (Gazzi–Dickinson method). Sand classification is based on the three main components (Q: quartz; F: feldspars; L: lithic fragments), considered if exceeding 10%QFL (e.g., a sand is named quartzo-lithic if L > Q > 10%QFL > F). Very low- to low-rank metamorphic rock fragments, for which protolith can still be inferred, were subdivided into metasedimentary (Lms) and metavolcanic (Lmv) categories. Medium- to high-rank metamorphic lithics were subdivided into felsic (metapelite, metapsammite and metafelsite; Lmf) and mafic (metabasite; Lmb) categories [*Garzanti and Vezzoli, 2003*].

From a split aliquot of the bulk sample or of a wide size-range obtained by sieving (mostly 32-500 μm), heavy minerals were separated by centrifuging in Na-polytungstate (2.90 g/cm^3) and recovered by partial freezing with liquid nitrogen; 200-250 transparent heavy minerals were counted on grain mounts. Heavy-mineral concentrations, calculated as the volume percentage of total (HMC) and transparent (tHMC) heavy minerals [*Garzanti and Andò 2007*], range from extremely poor (tHMC < 0.1) to extremely rich (tHMC ≥ 20). Significant minerals are listed in order of abundance throughout the text.

3.1. End-members

Each tectonic domain in the Taiwan orogen generates sediment with specific composition (Table 1; *Garzanti and Resentini, 2016*). Feldspatho-lithic sand derived from Luzon Arc andesites is dominated by microlitic to lathwork volcanic rock fragments and plagioclase, with little quartz, no K-feldspar, and rich clinopyroxene-hypersthene heavy-mineral suites with kaersutitic hornblende. Quartzo-feldspatho-lithic sand from the Tatun volcano includes biotite and extremely rich hypersthene-clinopyroxene suites with both kaersutitic hornblende and oxy-hornblende. Sand recycled from siliciclastic units of the Coastal Range is quartzo-lithic with abundant shale/slate to sandstone/metasandstone, a few cellular serpentinite, and rare metacarbonate and metabasite rock fragments. Poor heavy-mineral suites include hypersthene, epidote, clinopyroxene, hornblende, and minor zircon, apatite and Cr-spinel. The Lichi mélange sheds mudstone-dominated quartzo-lithic detritus associated with a very poor epidote-amphibole-pyroxene-garnet heavy-mineral suite.

Sand from the Yuli Belt is litho-quartzose metamorphiclastic with some feldspars (plagioclase > K-feldspar), abundant metapelite/metapsammite, subordinate metabasite, and minor serpentinite rock fragments. Rich heavy-mineral suites are dominated by amphibole and epidote. Sand shed by the Tailuko Belt is quartzo-lithic metamorphiclastic with paragneiss, schist, marble and metabasite rock fragments, and a few feldspars (plagioclase > K-feldspar). Moderately rich heavy-mineral suites are dominated by hornblende with subordinate epidote.

The Eocene Pilushan Formation exposed in the Backbone Range sheds quartzo-lithic metasedimentaclastic sand with dominant shale/slate rock fragments and a poor heavy-mineral suite consisting chiefly of chemically durable zircon, tourmaline, apatite and Ti oxides, associated with epidote, amphibole and few pyroxenes. Sand from the Miocene Lushan Formation is quartzo-lithic sedimentaclastic with a poor heavy-mineral assemblage dominated by zircon, tourmaline, apatite and rutile. Sand derived from the Hsuehshan Range Belt is quartzo-lithic metamorphiclastic, with abundant slate and metasandstone rock fragments and a poor, zircon-tourmaline heavy-mineral assemblage.

Sand recycled from the Inner Western Foothills is quartzo-lithic sedimentaclastic with abundant shale/slate, siltstone, sandstone/metasandstone rock fragments. Poor heavy-mineral suites include zircon, garnet, tourmaline, epidote, rutile and apatite. A similar heavy-mineral assemblage characterizes detritus from the Outer Western Foothills, shedding feldspatho-litho-quartzose sand with limestone, felsitic volcanic and chert rock fragments occur.

3.2. Major rivers

Most major rivers of Taiwan are sourced in the Slate Belt, representing the backbone of the orogen. Sediment composition, however, is distinctly different in western Taiwan rivers cutting transversally across the pro-wedge, and in eastern Taiwan rivers draining the retro-wedge and flowing parallel to the Longitudinal Valley Fault for long tracts. Sands of western Taiwan rivers range from quartzo-lithic metasedimentaclastic to litho-quartzose sedimentaclastic. Lithic shale/slate sand shed from the Slate Belt mixes progressively downstream with quartz, feldspar and garnet recycled from Neogene siliclastic units exposed in the Western Foothills. Sands of eastern Taiwan rivers are more varied. Quartzo-lithic metasedimentaclastic Lanyang sand is derived chiefly from the Backbone and Hsuehshan Ranges. Instead, litho-quartzose metamorphiclastic to quartzo-lithic metasedimentaclastic sands carried by the Hualian, Xiuguluan and Beinan Rivers are derived in various proportions from the Tailuko and Yuli Belts of the Tananao metamorphic complex, from andesites and overlying Plio-Pleistocene siliciclastic rocks of the Coastal Range, and from the Backbone Range.

Table 1. Petrographic and mineralogical signatures of detritus from the diverse tectono-stratigraphic units of the Taiwan orogen and from major rivers

	end-members	# samples	HMC % PTHM	tHMC % PTHM	SRD PTHM	MI	Q	F	Lv	Lc	Ls	Lms	Lmv	Lmf	Lmb	Lu	mica	opaques	turbid	zircon	tourmaline	rutile	titanite	apatite	epidote	garnet	chloritoid	staurolite	Al silicates	amphibole	pyroxene	spinel	total
Coastal Range	Volcanics	2	6.9	6.5	2.73	3	2	25	63	0	2	0	1	0	0	0	0.0	0.4	0.0	0.0	0.0	0.0	0.0	0.0	0.0	0.0	0.0	0.0	0.0	0.3	6.2	0.0	*100*
			4.4	*4.3*	*0.03*	*1*	*1*	*7*	*11*	*0*	*1*	*1*	*0*	*0*	*0*	*0*	*0.0*	*0.1*	*0.0*	*0.0*	*0.0*	*0.0*	*0.0*	*0.0*	*0.0*	*0.0*	*0.0*	*0.0*	*0.0*	*0.2*	*4.4*	*0.0*	
	Sedimentary	2	1.0	0.7	2.60	42	38	5	3	3	31	16	0	0	0	1	0.0	0.2	0.0	0.0	0.0	0.0	0.0	0.0	0.1	0.0	0.0	0.0	0.0	0.1	0.4	0.0	*100*
			0.5	*0.3*	*0.03*	*37*	*4*	*0*	*0*	*2*	*10*	*13*	*0*	*1*	*0*	*1*	*0.0*	*0.1*	*0.0*	*0.0*	*0.0*	*0.0*	*0.0*	*0.0*	*0.1*	*0.0*	*0.0*	*0.0*	*0.0*	*0.1*	*0.2*	*0.0*	
	Lichi Fm.	1	0.4	0.2	2.50	22	15	2	2	1	65	13	0	1	0	0	0.0	0.2	0.0	0.0	0.0	0.0	0.0	0.0	0.1	0.0	0.0	0.0	0.0	0.0	0.0	0.0	*100*
Tananao Complex	Yuli Fm.	2	8.7	7.5	2.74	216	44	6	0	2	8	8	2	20	1	1	0.4	1.1	0.1	0.0	0.0	0.0	0.1	0.2	3.8	0.0	0.0	0.0	0.0	3.4	0.0	0.0	*100*
			6.2	*6.6*	*0.08*	*74*	*17*	*3*	*1*	*0*	*9*	*6*	*2*	*7*	*2*	*0*	*0.6*	*0.3*	*0.2*	*0.0*	*0.0*	*0.0*	*0.1*	*0.1*	*4.8*	*0.0*	*0.0*	*0.0*	*0.0*	*1.6*	*0.0*	*0.0*	
	Tailuko Fm.	4	9.4	8.0	2.78	299	30	7	0	21	1	6	3	20	2	0	0.7	1.1	0.2	0.1	0.0	0.0	0.1	0.2	4.3	0.0	0.0	0.0	0.0	3.4	0.0	0.0	*100*
			5.8	*5.7*	*0.03*	*46*	*6*	*6*	*0*	*7*	*1*	*4*	*4*	*9*	*2*	*0*	*0.8*	*0.4*	*0.2*	*0.1*	*0.0*	*0.0*	*0.1*	*0.1*	*3.0*	*0.0*	*0.0*	*0.0*	*0.0*	*3.2*	*0.0*	*0.0*	
Central Range	Eocene	1	3.9	3.2	2.69	131	17	1	0	0	15	55	0	8	0	0	0.0	0.3	0.0	0.7	0.8	0.1	0.0	0.5	0.6	0.0	0.0	0.0	0.0	0.3	0.1	0.0	*100*
	Miocene	10	1.2	0.3	2.57	49	13	1	0	1	48	35	0	1	0	0	0.0	0.8	0.0	0.1	0.1	0.0	0.0	0.0	0.0	0.0	0.0	0.0	0.0	0.0	0.0	0.0	*100*
			0.4	*0.1*	*0.06*	*28*	*5*	*1*	*0*	*1*	*18*	*17*	*0*	*1*	*0*	*0*	*0.0*	*0.3*	*0.0*	*0.1*	*0.0*	*0.0*	*0.0*	*0.0*	*0.0*	*0.0*	*0.0*	*0.0*	*0.0*	*0.0*	*0.0*	*0.0*	
	Hsuehshan	2	2.8	1.1	2.68	93	26	2	0	0	19	49	0	1	0	0	0.0	1.3	0.0	0.5	0.5	0.0	0.0	0.0	0.1	0.0	0.0	0.0	0.0	0.0	0.0	0.0	*100*
			0.2	*1.1*	*0.05*	*34*	*4*	*1*	*0*	*0*	*11*	*14*	*0*	*2*	*0*	*0*	*0.0*	*0.9*	*0.0*	*0.5*	*0.5*	*0.0*	*0.0*	*0.0*	*0.0*	*0.0*	*0.0*	*0.0*	*0.0*	*0.0*	*0.0*	*0.0*	
Western foothills	Inner	1	3.4	1.9	2.64	49	34	6	1	0	33	23	0	0	0	0	0.3	1.5	0.0	0.5	0.4	0.1	0.0	0.2	0.2	0.4	0.0	0.0	0.0	0.1	0.0	0.0	*100*
	Outer	2	0.9	0.6	2.65	69	65	14	3	1	7	6	0	1	0	0	0.4	0.2	0.0	0.2	0.1	0.0	0.0	0.1	0.1	0.1	0.0	0.0	0.0	0.0	0.0	0.0	*100*
			0.3	*0.3*	*0.02*	*41*	*2*	*0*	*1*	*1*	*4*	*3*	*0*	*0*	*0*	*0*	*0.2*	*0.0*	*0.0*	*0.1*	*0.1*	*0.0*	*0.0*	*0.0*	*0.0*	*0.0*	*0.0*	*0.0*	*0.0*	*0.0*	*0.0*	*0.0*	
Major rivers																																	
River	**Site**																																
Dahan	Sanying		1.0	0.3	2.61	113	64	6	2	0	24	3	0	0	0	0	0.3	0.6	0.0	0.1	0.0	0.0	0.0	0.0	0.1	0.1	0.0	0.0	0.0	0.0	0.1	0.0	*100*
Xindian	Xindian		0.8	0.2	2.50	104	12	2	1	0	71	14	0	0	0	0	0.0	0.6	0.0	0.0	0.0	0.0	0.0	0.0	0.0	0.0	0.0	0.0	0.0	0.0	0.2	0.0	*100*
Lanyang	Erjie		1.4	0.2	2.61	128	21	1	3	2	34	37	0	1	0	0	0.3	0.9	0.1	0.1	0.0	0.0	0.0	0.0	0.0	0.0	0.0	0.0	0.0	0.0	0.0	0.0	*100*
Heping	Heping		7.8	3.2	2.79	204	29	5	0	4	8	31	4	12	1	0	0.3	4.1	0.1	0.0	0.0	0.0	0.0	0.2	1.8	0.1	0.0	0.0	0.0	1.0	0.0	0.0	*100*
Liwu	Tailuko		3.2	1.1	2.70	220	34	4	1	10	15	18	3	10	1	0	0.6	2.1	0.0	0.0	0.0	0.0	0.0	0.0	0.5	0.0	0.0	0.0	0.0	0.5	0.0	0.0	*100*
Hualian	Renhe		5.1	2.5	2.77	309	42	4	1	10	2	6	1	29	1	0	0.0	2.4	0.0	0.0	0.1	0.0	0.1	0.0	0.8	0.0	0.0	0.0	0.0	1.2	0.2	0.0	*100*
Xiuguluan	Dagangkou		6.8	5.3	2.74	292	43	8	5	6	6	8	1	13	1	0	1.4	1.2	0.1	0.1	0.1	0.0	0.1	0.1	2.5	0.0	0.0	0.0	0.0	1.4	1.1	0.0	*100*
Beinan	Chishang		3.0	1.7	2.66	214	19	5	2	6	24	24	4	13	0	0	0.0	1.2	0.0	0.1	0.0	0.0	0.0	0.1	1.2	0.0	0.0	0.0	0.0	0.3	0.0	0.0	*100*
Kaoping	Daliao		1.5	0.5	2.55	132	15	1	1	2	58	20	0	1	0	0	0.0	0.9	0.0	0.2	0.1	0.0	0.0	0.0	0.0	0.0	0.0	0.0	0.0	0.0	0.0	0.0	*100*
Tsengwen	Xigang		1.1	0.9	2.61	150	61	6	2	6	23	1	0	0	0	0	0.0	0.1	0.1	0.2	0.2	0.1	0.0	0.1	0.1	0.1	0.0	0.0	0.0	0.0	0.1	0.0	*100*
Bazhang	Haomeiliao		0.7	0.4	2.64	136	66	14	3	1	10	4	0	1	0	0	0.3	0.2	0.0	0.1	0.0	0.0	0.0	0.1	0.1	0.1	0.0	0.0	0.0	0.0	0.0	0.0	*100*
Zhuoshui	Dacheng		0.7	0.4	2.56	133	33	3	0	2	44	15	0	1	0	0	0.0	0.3	0.0	0.1	0.0	0.0	0.0	0.0	0.0	0.1	0.0	0.0	0.0	0.0	0.0	0.0	*100*
Dadu	Longjing		1.9	1.0	2.60	100	45	4	1	1	37	11	0	0	0	0	0.3	0.7	0.0	0.4	0.2	0.1	0.0	0.1	0.1	0.1	0.0	0.0	0.0	0.0	0.0	0.0	*100*
Dajia	Qingshui		0.9	0.4	2.59	136	55	5	2	0	32	5	0	0	0	0	0.0	0.5	0.0	0.1	0.1	0.0	0.0	0.0	0.1	0.0	0.0	0.0	0.0	0.0	0.0	0.0	*100*
Da'an	Da'an		1.4	0.6	2.58	100	54	2	2	0	39	2	0	0	0	0	0.0	0.8	0.0	0.2	0.2	0.0	0.0	0.0	0.1	0.1	0.0	0.0	0.0	0.0	0.0	0.0	*100*
245 Touqian	Xizhou		1.5	0.8	2.55	103	31	6	3	0	50	8	1	0	0	0	0.0	0.7	0.1	0.1	0.0	0.0	0.0	0.1	0.0	0.0	0.0	0.0	0.0	0.0	0.4	0.0	*100*

Table 1: Petrographic and mineralogical signatures of detritus derived from the diverse tectono-stratigraphic units of the Taiwan orogen and carried by major rivers. HMC and tHMC: total and transparent Heavy Mineral Concentration indices; SRD: Source Rock Density index (g/cm^3); MI: Metamorphic Index; Q: quartz; F: feldspar; L: lithic grains (Lv: volcanic; Lc: carbonate; Ls: other sedimentary; Lms: very low-rank to low-rank metasedimentary; Lmv: very low-rank to low-rank metavolcanic; Lmf: medium-rank to high-rank metapsammite/metafelsite; Lmb: medium-rank to high-rank metabasite; Lu: ultramafic). Average and standard deviations are given for end-member compositions of two or more samples.

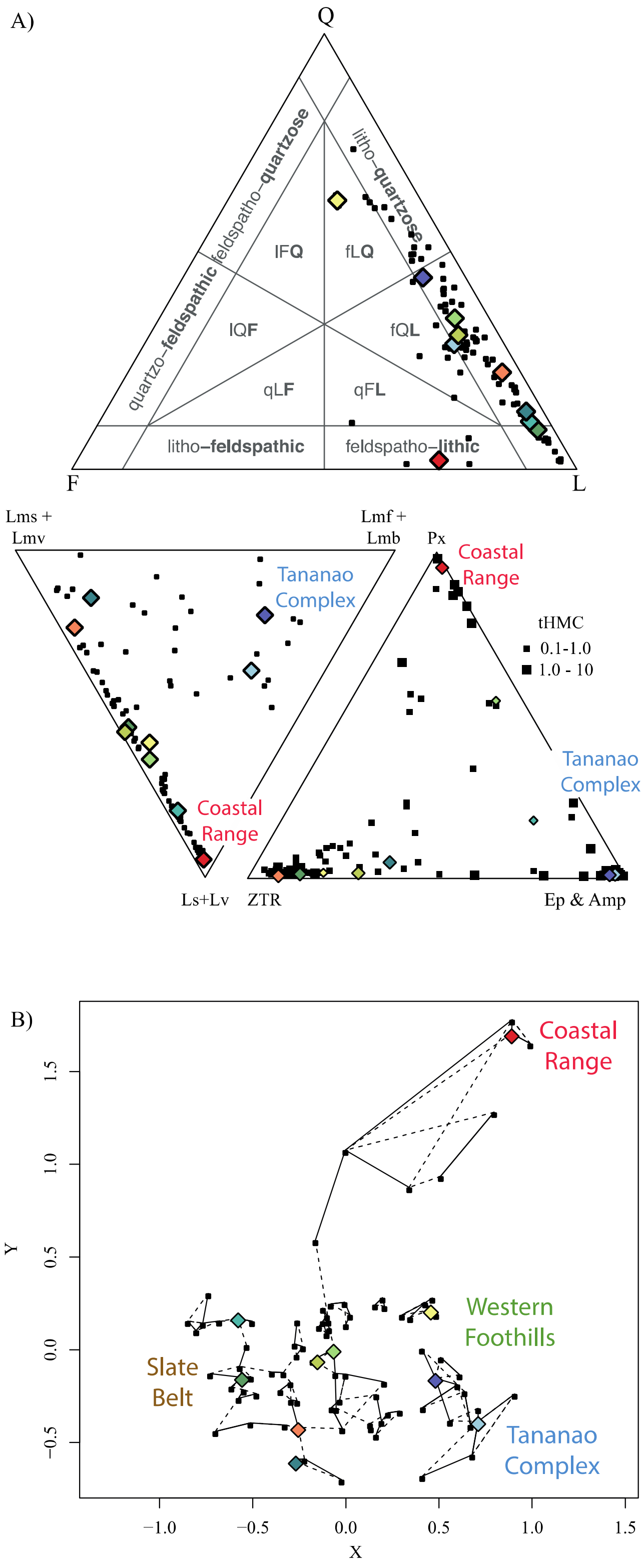

Figure 3: Detrital signatures of modern river sands from Taiwan. A) QFL diagram (top; classification after Garzanti 2016) and triangular diagrams for lithic grains (left) and heavy minerals (right). ZTR: zircon, tourmaline and rutile; Ep: epidote; Amp: amphibole; Px: pyroxene. Other parameters as in Table 1. B) Multidimensional Scaling map [*Vermeesch et al., 2016*] of the Taiwan compositional dataset, representing petrographic and heavy-mineral data in a single graph. Samples with similar composition plot

close together; for each sample the contribution from the different end-members is inversely proportional to their statistical distance. Color scheme as in Figure 1.

4. PARTITIONING THE SEDIMENT FLUX

4.1. Provenance budget

4.1.1. Rationale

Terrigenous detritus reaching the closure section of a drainage basin consists of a complex mixture of single minerals and rock fragments supplied by the geological units exposed in the drainage basin. If the end-member compositional signatures of source units are known, then the relative contributions to the total sediment flux from each source can be mathematically quantified with forward mixing models [*Draper and Smith, 1998*; *Weltje, 1997*].

Compositional data are closed data where each variable (D) represents its relative contribution to a whole. The sample space for compositional data is not the real space R^D, but the simplex S^D [*Aitchison, 1986*]:

$$(1) \qquad S^D = \left\{ x = [x_1, x_2, \ldots, x_D]; \qquad x_i > 0; \qquad i = 1,2,\ldots,D; \qquad \sum_{i=1}^{D} x_i = c \right\}.$$

where x represents a composition consisting of D variables. The sum of all variables in each observation (sample) is constant (c), and all variables are greater than 0.

In order to satisfy the positive-variable constraint, all zeros hosted in the compositional dataset were replaced by amalgamation and/or application of a multiplicative replacement strategy [*Martin-Fernandez et al., 2003*]:

$$(2) \qquad \overline{x_j} = \begin{cases} \delta_j & if\ x_j = 0 \\ \left(1 - \frac{\sum_{k|x_k=0} \delta_c}{c}\right) & if\ x_j > 0 \end{cases}$$

where δ_j is the input value (0.0025, in our case).

4.1.2. The mixing model

A D-part composition (y) can be expressed as the result of mixing in various proportions of n end-member compositions (X = n × D):

$$(3) \qquad y = \beta X + e$$

where β is the vector of the mixing proportions and e is the error vector.

The constraints for equation (3) are:

$$(4) \qquad \sum_{k=1}^{n} b_k = 1; \qquad b_k \geq 0$$

For each river basin, the composition of detritus derived from each single geological unit exposed was considered as an end-member. To identify the best-fit mixing proportions we simulated all possible combinations of the potential end-members, and measured subsequently the similarity between the observed (x_i) and each modelled (x_j) composition. All possible combinations of the end-members were performed at steps of 5%, leading to a minimum of 21 modelled compositions for 2 end-members to a maximum exceeding 10^7 for 10 end-members. Goodness of fit was assessed both by the Aitchison distance:

$$(5) \qquad \sqrt{\sum_{k=1}^{D}\left(\log\left(\frac{x_{ik}}{g(x_i)}\right)-\log\left(\frac{x_{jk}}{g(x_j)}\right)\right)^2}$$

where g is the geometric mean of the compositional data, and by the Euclidean distance:

$$(6) \qquad \sqrt{\sum_{k=1}^{D}\left(x_{ik}-x_{jk}\right)^2}\,.$$

4.1.3. Sources of uncertainty

The unmixing process involves diverse assumptions. To quantify the contribution from the different end-members to the observed composition of a fluvial sediment, end-members should be linearly independent and sufficiently diverse compositionally to produce unambiguous results. In this study, the detrital signatures of the 10 main tectono-stratigraphic units of Taiwan were chosen as end-members. The differences among end-members were assessed by the Aitchison distance (Table 2) and by multidimensional scaling maps (Figure 3).

End-member compositions must fulfil three assumptions.

First, sediment samples collected from a few small streams draining a single tectono-stratigraphic unit (*first order sampling scale* of *Ingersoll et al., 1993*) must be representative of the entire parent unit. Because accuracy increases with the number of replicate samples, up to 10 sediment samples were used for a single unit where available. In these cases (e.g., Miocene of the Slate Belt), the coefficients of variations are low and the average compositional parameters are robust. However, only one sample could be used to characterize the Eocene of the Slate Belt, the Oligocene to Pleistocene strata of the Inner Western Foothills, and the Pliocene Lichi mélange.

Second, the composition obtained from a sand sample collected at the outlet of a river basin should represent accurately the composition of the sediment generated in the entire basin. Reproducibility was tested wherever replicates were available; the statistical difference among replicates resulted to be generally low (Aitchison Distance 4.3±0.4 and 4.2±0.7 for Tsengwen and Zhuoshui samples).

Table 2: Aitchison distances among Taiwan end members

		Coastal Range			Tananao Complex		Central Range			Western foothills	
		Volcanics	Sedimentary	Lichi Fm.	Yuli Fm.	Tailuko Fm.	Eocene	Miocene	Hsuehshan	Inner	Outer
Coastal Range	Volcanics	*0*	5.6	6.4	8.2	9.1	8.9	7.4	8.5	7.8	7.1
	Sedimentary	5.6	*0*	4.3	5.2	6.2	7.1	5.1	6.0	6.9	5.7
	Lichi Fm.	6.4	4.3	*0*	5.8	6.2	6.0	4.1	5.1	6.4	5.0
Tananao Complex	Yuli Fm.	8.2	5.2	5.8	*0*	3.0	7.6	5.8	6.6	7.6	5.7
	Tailuko Fm.	9.1	6.2	6.2	3.0	*0*	7.5	6.2	6.2	8.2	6.2
Central Range	Eocene	8.9	7.1	6.0	7.6	7.5	*0*	5.9	4.2	6.4	6.8
	Miocene	7.4	5.1	4.1	5.8	6.2	5.9	*0*	3.6	5.0	3.5
	Hsuehshan	8.5	6.0	5.1	6.6	6.2	4.2	3.6	*0*	5.5	5.0
Western foothills	Inner	7.8	6.9	6.4	7.6	8.2	6.4	5.0	5.5	*0*	4.5
	Outer	7.1	5.7	5.0	5.7	6.2	6.8	3.5	5.0	4.5	*0*

Table 2: Aitchison distances among end-member compositions. Discrimination of different end-member sources is more robust for larger Aitchison distances.

Third, sediment composition depends primarily on the lithology of source rocks, but may reflect also a complex combination of physical and chemical effects produced during erosion, transport, and deposition. Landslides induced by frequent earthquakes and typhoons indicate dominantly physical erosion with only moderate weathering processes in the island of Taiwan, where temperature and rainfall are consistently high and rather homogeneously distributed [*Garzanti and Resentini, 2016*]. Hydraulic-sorting effects, which can alter severely sediment composition by selectively enrichment or depletion of specific detrital species according to their size and density, were checked and corrected for by monitoring the HMC and SRD parameters [*Garzanti and Andò, 2007*; *Garzanti et al., 2009*]. The HMC and SRD values are generally low in our river samples (3±3 and 2.64±0.08, respectively), the only exception being represented by volcaniclastic sands derived from the Tatun Volcano (45±9 and 3.23±0.13). Heavy-mineral enrichment by selective-entrainment effects is thus negligible. Diagenetic modifications are null in modern sands.

To account for the uncertainties associated with these three assumptions, and bearing in mind that the geological complexity of natural processes may depart substantially from theory, we performed independent trials with replicate samples. For each sample, the best solutions was selected as the set of mixing proportions yielding a maximum statistical distance of 120% of the minimum for both Aitchison and Euclidean methods. The average (μ) and the standard deviation (σ) of such a set of solutions were used to calculate our provenance budget and the associated uncertainties (Figure 4). All results were checked for geological significance, and geologically meaningless solutions were discarded.

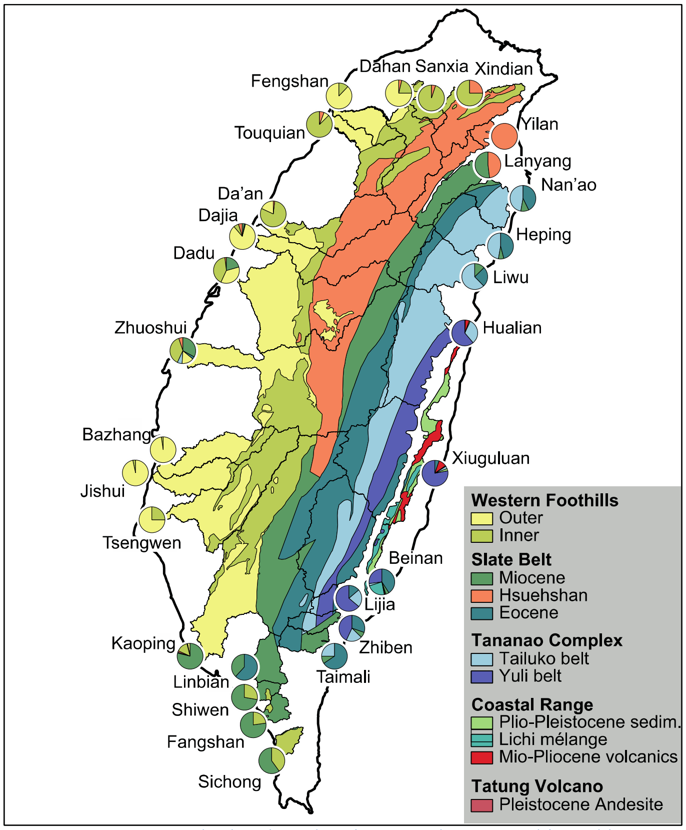

Figure 4: Provenance budget based on integrated petrographic and heavy-mineral data. Color scheme as in Figure 1.

4.2. Sediment budget

4.2.1. Rationale

A provenance budget estimates the relative contributions from different parent sources (e.g., catchments or tectonic domains) to a daughter sediment. If a reliable estimate of the sediment flux [Mt a^{-1}] is available, then it can be partitioned among the different sources according to such relative contributions, and a sediment budget is obtained. The sediment yield [t a^{-1} km^{-2}] from a given source can be calculated next as the ratio between the sediment flux and the area of the source, as deduced from the geological map (in our case the *Central Geological Survey MOEA,* *2000*). Erosion rates for each source [mm/a] can be finally calculated as the ratio between the sediment yield and average density of exposed rocks [g/cm^3].

Because solutions can be far from unique, erosion rates were calculated using the maximum and minimum contributions from each source to the provenance budget (μ+σ and μ-σ, respectively). The mean and standard deviation of all results were used to assess erosion rates and the associated uncertainties for each unit in each catchment. Finally, erosion rates were smoothed by calculating the average value in adjacent polygons within the same geological unit.

4.2.2. Sources of uncertainty

The major source of uncertainty by far in the calculation of provenance-derived erosion rates is the lack of robustness of sediment-load data. The suspended load of a river is usually calculated by measuring sediment concentration multiplied by time-weighted water discharge [*Porterfield, 1972*]. Such estimates, based on regression analysis, may be subject to significant errors also because of the limited temporal resolution of the data [*Glysson et al., 2001*]. Moreover, suspended sediment fluxes should be integrated through the entire horizontal and vertical profile of the river channel [*Bouchez et al., 2001*; *Lupker et al., 2011*]. Last but not least, solid-load data are usually limited to the suspended fraction, due to the impossibility of measuring bedload directly, particularly during floods. The dataset used in this study is a compilation of sediment fluxes from Table S1 in Dadson et al. [2003], integrated with data from Hwang [1982] and Liu et al. [2008]. All three sources report only suspended load for Taiwan rivers, recorded over time spans ranging from 1 to 31 years and largely based on hydrological data from the Water Resources Agency, Ministry of Economic Affairs. Mean variations of suspended-load estimates among the three datasets are ~70% of the average, with a maximum of 146% in the Nan'ao catchment. For each gauging station, the annual variability corrected for seasonal effects was calculated to be 36%, reaching up to 95% for the upper Houlong catchment.

Rather than on suspended load, which is too fine-grained for petrographic analysis, our provenance budget is based on the composition of bedload sand. The suspended/bedload ratio is an unsolved issue in fluvial sedimentology, and changes in space and time according to flow regime, riverbed composition, rock strength and upstream drainage area [*Maddock and Borland, 1950*; *Pratt-Sitaula et al., 2007*; *Turowski et al., 2010*]. Based on the considerations illustrated at the beginning of section 6, we have investigated two different scenarios, with suspended/bedload ratios 70/30 and 90/10. If the assumed suspended/bedload ratio is too low, then the estimated erosion rates are too high, and vice versa. The relative values, however, remain unchanged. If we consider that the suspended/bedload ratio increases as relief and river competence decrease, then our erosion rates would be too high in the lowlands (e.g., Outer Western Foothills), and too low in the highlands. In the absence of bedload data, we cannot explore the scenario where the suspended/bedload ratio changes downstream, but we can test the likelihood of our assumptions if the results are cross-checked with independent geomorphological approaches (see section 5 below). Another assumption is that the mud/sand generation potential is the same for all lithologies, which is clearly an oversimplification (e.g., granites and sandstones generate more sand, slate and shales more mud). As a consequence, erosion rates tend to be too high for coarse-grained tectosilicate-rich rocks and too low for fine-grained phyllosilicate-rich rocks. In the absence of independent data, any ad hoc criterion aimed at solving this thorny problem would inevitably suffer from circular reasoning.

Further problems are associated with the measurement of catchment areas used to calculate sediment yields. Because areas are measured on a map, the effect of slope is not taken into account. Vertical cliffs are not represented in plan view, and areas of units exposed on steep slopes are systematically underestimated. As a consequence, sediment yield from units exposed in steep mountain regions tend to be overestimated. If we correct the area of each end-member unit according to its mean slope in each river catchment [$area_{corrected} = area_{planview} / \cos(slope)$], then we obtain a maximum increase of 10±4% for the area of the Tailuko unit, a minimum increase of 4±4% for the Outer Foothills, and corresponding decreases in sediment yield and erosion rates.

Finally, we need to choose a convenient average density for each tectono-stratigraphic unit. Based on our extensive petrographic and mineralogical dataset on modern sands, we could determine a reliable value for each source rock (SRD indices in Table 1), under the acceptable assumption of negligible physical and chemical effects during erosion, transport and deposition (as discussed above in section 4.1.3).

Table 3: Mean annual erosion rates (mm/a)

	Bedload: 30% of total sediment load										Bedload: 10% of total sediment load									
	Coastal Range			Tananao Complex		Central Range			Western foothills		Coastal Range			Tananao Complex		Central Range			Western foothills	
Drainage basin	Volcanics	Sedimentary	Lichi Fm.	Yuli Fm.	Tailuko Fm.	Eocene	Miocene	Hsuehshan	Inner	Outer	Volcanics	Sedimentary	Lichi Fm.	Yuli Fm.	Tailuko Fm.	Eocene	Miocene	Hsuehshan	Inner	Outer
Dahan								2.5	1.9	5.2								1.2	1.5	4.0
Sanxia								0.4	2.6									0.3	2.1	
Xindian								3.7	3.6									4.1	2.8	
Yilan								5.9										4.7		
Lanyang							9.5	3.6									6.4	4.8		
Nan'ao					6.9	15.4	12.5								5.4	11.9	11.2			
Heping					7.9	9.7	9.5								7.0	8.4	6.4			
Liwu					8.9	6.3	23.6								6.9	3.3	14.0			
Haulian	33.3	1.3		29.7	23.4	3.3					26.7	1.0		23.1	19.3	2.3				
Xiuguluan	9.7	1.3	7.1	45.2	23.4	7.3					7.5	1.0	5.5	37.0	19.3	7.8				
Beinan			7.2	38.6	6.6	8.9	37.5						5.5	30.7	5.7	8.7	29.2			
Lijia				42.0	8.3	15.6								31.9	6.2	11.3				
Zhiben				24.9	10.1	5.9	1.3							19.4	7.5	3.5	1.0			
Taimali					11.6	27.9	1.3								9.0	12.9	1.0			
Sichong							-		1.2								-		1.0	
Fangshan							2.7		7.9								2.1		6.1	
Shiwen							2.7		7.9								2.1		6.1	
Linbian						32.7	8.3									14.8	8.3			
Donggang							10.1										8.0			
Kaoping					8.3	27.4	19.2	3.4	9.3	1.1					6.2	17.9	17.6	2.6	7.5	0.8
Tsengwen									7.3	9.4									6.0	7.3
Jishui									3.6	8.8									2.8	7.5
Bazhang									1.8	5.1									1.4	3.9
Zhuoshui					27.9	2.4	22.3	2.3	10.0	4.0					22.0	1.9	16.6	1.7	8.9	3.1
Dadu							10.7	0.8	10.1	5.1							9.3	0.7	6.5	4.6
Dajia						9.9	19.9	3.3	11.0	4.5						7.4	13.9	1.5	6.2	4.0
Da'an								0.2	10.6	5.8								0.1	8.3	4.5
Touqian								0.2	1.5	1.1								0.1	1.4	0.9
Fengshan									1.5	3.6									1.5	3.0

Table 3: Mean annual erosion rates (mm/a) calculated for different tectono-stratigraphic units exposed in different catchments. Estimates were smoothed by calculating the average value in adjacent polygons within the same geological unit. Results based on suspended/bedload ratios of 70/30 and 90/10 are shown.

5. GEOMORPHOLOGY

We compared the provenance-derived erosion rates $E_p(u)$ - where $_p$ stands for provenance and u refers to the erosion rate of each tectono-stratigraphic unit in each basin - to morphometric proxies of erosion rates. We assume that the morphometry-derived erosion rate $E_m(u)$ is controlled by channel incision, which by itself can be expressed using the stream-power model:

$$(7) \qquad E_m = K(u)Q(u)^m S(u)^n$$

where $Q(u) = \sum \Delta A(u)P(u)$, A [km^2] is the upstream drainage area and P [mm/a] the annual precipitation. S is the slope, and K [mm^{1-3m}/a^{1-m}] the erodibility, which reflects both the hydraulic properties of the fluvial channel and the mechanical properties of the bedrock (i.e., its susceptibility to erosion). The powers m and n are empirical positive constants (m= 0.5, n= 1; *Whipple and Tucker, 1999*), and x represents an ad hoc coordinate system along the fluvial channel. Because K is unknown, we calculate the Erosion Index EI = E_m/K [*Finlayson et al. 2002*]:

$$(8) \qquad EI = Q(u)^m S(u)^n$$

where we consider fluvial drainage network pixels that drain an area > 10 km^2. The fluvial network was extracted from a 1 arcsec SRTM digital elevation model, and precipitation data were extracted from Water Resource Agency, Ministry of Economic Affairs, Taiwan (*http://eng.wra.gov.tw*). Next, EI(u) was calculated as the mean over all EI(u) values for all pixels belonging to each tectono-stratigraphic unit in each basin containing more than 130 river-channel pixels. We note that the erosion index is related to the steepness index k_s [*Wobus et al. 2006*] via EI = k_s^n.
The erodibility (K) can be calculated by minimizing the mean least square of the correlation between $E_p(u)$ and EI(u) for all units in all basins. A more robust correlation is obtained by considering only $E_p(u)$ values < 10 mm/a (for suspended/bedload ratio 90/10), and < 15 mm/a (for suspended/bedload ratio 70/30). The erodibility value K^* was thus obtained for each tectono-stratigraphic unit; an indicative average $\overline{K}$ value for the entire Taiwan orogen was also calculated. By comparing the reciprocal of erodibility values K^* to rock-strength data from Table S3 in Dadson et al. [2003] we obtained a monotonic linear correlation between $1/K^*$ and the square of the tensile strength (Figure 5). Such a correlation has been predicted by an abrasive mill experiment [*Sklar and Dietrich, 2001*], but was never directly inferred from field data so far.

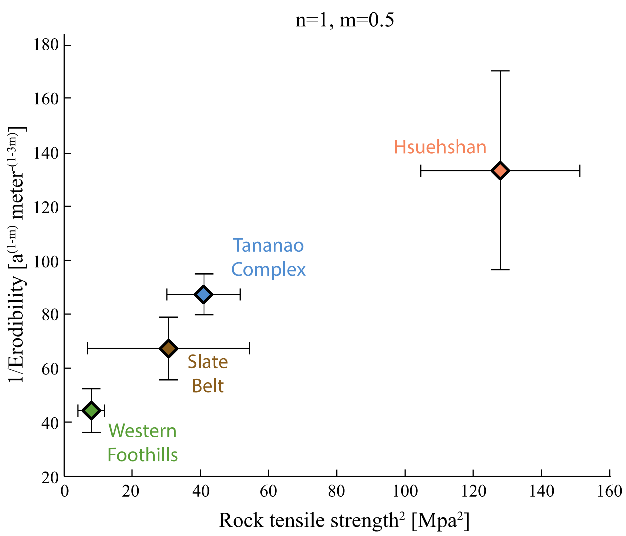

Figure 5: Correlation between the square of rock tensile strength estimated from Table S3 in Dadson et al. [2003] and the reciprocal of the erodibility as inferred from the correlation between $E_p(u)$ and EI(u). Error bars represent one standard deviation. Tensile strength is estimated based on Mohr-Coulomb failure envelop for the relation between uniaxial compressive strength and the cohesion, C, assuming an angle of internal friction of 30°. Griffith theory is used to relate C to the tensile strength T as T= C/2. This calculation resulted in $T = 0.1415\sigma_c$, where σ_c is the uniaxial compressive strength as reported in Dadson et al. (2003). The suspended/bedload ratio is assumed to be 70/30 and only tectono-stratigraphic unit in each basin with erosion rates <15 mm/a have been considered.

Finally, erosion rates for each tectono-stratigraphic unit in each basin were calculated using individual erodibility values for each unit as $E_m(u) = K^* EI(u)$ (Figure 6).

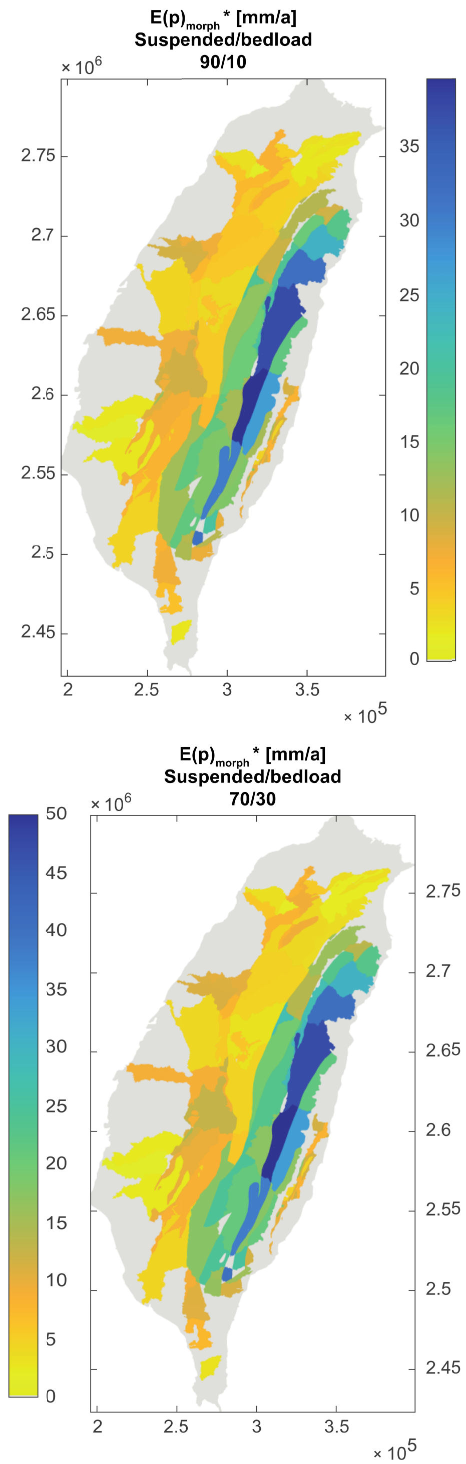

Figure 6: Morphometry-derived erosion rates under the assumption of suspended/bedload ratios of 90/10 (top) and 70/30 (bottom). Erosion rates are calculated using different erodibility values (K^{*}) for each tectono-stratigraphic unit as explained in text.

6. TRACING EROSION PATTERNS

The most crucial assumption for the determination of provenance-derived erosion rates regards the suspended/bedload ratio. According to Dadson et al. [2003 p.648], "*suspended sediment and bedload comprise about 70±28% and 30±28%, respectively, of total river load in high mountains (uncertainties are 95% confidence intervals)*". Dadson et al. [2003], however, ignored bedload in their calculation of erosion rates based on sediment fluxes, which as a consequence were underestimated systematically. Taking into account that generally "*the bed load is assumed to be about 10% of the suspended load"* [*Hay 1998* p.297], in this study of mountain rivers of Taiwan we used two different suspended/bedload ratios, of 70/30 and 90/10, to calculate total sediment loads from the suspended-load data available in the literature [*Hwang, 1982*; *Dadson et al., 2003*].

In order to smooth out the irregular spatial variability resulting from various sources of error, the provenance-derived erosion rates given below and in Figure 7 are averaged among adjacent sub-basins belonging to the same tectono-stratigraphic unit.

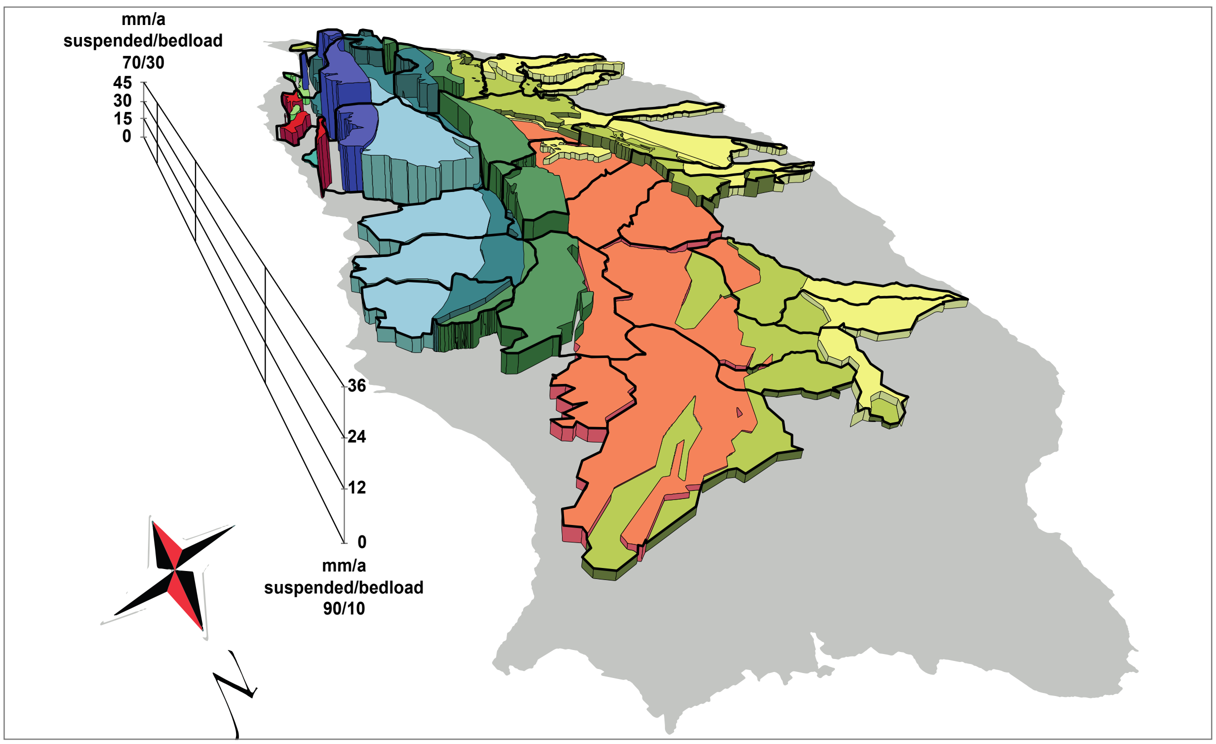

Figure 7: Perspective view of provenance-derived erosion rates.

6.1. Erosion along the retro-wedge

Very high erosion rates are estimated for the Yuli Belt (36.1±8.5 and 28.4±7.1 mm/a for suspended/bedload ratios of 70/30 and 90/10, respectively) and remain rather constant from north to south (Figure 7). The estimated rates for the Tailuko Belt are low in the north (7.9±1.0 and 6.4±0.9 mm/a; Nan'ao, Heping and Liwu catchments), increase sharply in central Taiwan (24.9±2.6 mm/a and 20.2±1.5; Hualian and Xiuguluan catchments), and drop again in the south (9.0±1.9 and 6.9±1.4 mm/a; Beinan, Lijia, Zhiben and Taimali catchments).

Our estimates are more variable and less robust for Coastal Range units. Erosion rates are estimated to be relatively low for the Lichi Mélange (7.1 and 5.5 mm/a) and very high for volcanic units (21.5 and 17.1 mm/a). Values for Plio-Pleistocene units, only a limited area of which is characterized by our samples, are even less constrained, their estimated contribution to the provenance budget having standard deviations up to 100% of the mean.

6.2. Erosion along the pro-wedge

Eocene to Miocene strata of the Backbone Range are estimated to be eroded more rapidly than the Hsuehshan Range to the west. Erosion rates are estimated to increase from the northern and central parts of the Eocene Slate Belt (7.8±4.4 and 6.2±3.7 mm/a) to its southern part (19.7±11.1 and 11.5±5.0 mm/a), where the highest values characterize the Linbian and Kaoping catchments (30.0±3.8 and 16.4±2.2 mm/a). A diversified erosion pattern is shown by the Miocene Lushan Formation. Rates increase from basins draining eastwards in the north (10.5±1.8 and 8.0±2.8 mm/a; Lanyang, Nan'ao and Heping catchments) to basins of central Taiwan (19.1±5.8 and 13.5±3.0 mm/a; Dajia, Liwu, Dadu and Zhuoshui catchments), and become more variable in the south (18.8±13.4 and 15.8±10.0 mm/a; Kaoping, Beinan, Donggang and Linbian catchments). Low values were obtained for the Hsuehshan Range (2.7 and 2.1 mm/a) and even lower rates for the Henchung Peninsula (< 1 mm/a). The Inner Foothills are characterized by rates lower in the north (2.2±0.9 and 1.8±0.6 mm/a), and higher elsewhere (7.6±3.2 and 5.7±2.4 mm/a). Similar values are obtained for the Outer Foothills (5.6±3.5 and 4.5±2.8 mm/a), with higher erosion rates in the Jishui and Tsengwen catchments (10.6±2.6 and 8.5±1.2 mm/a).

6.3. Comparison of provenance-derived versus morphometry-derived erosion rates

For each unit *u*, we calculated the mismatch between provenance-derived and morphometry-derived erosion rates as $E_p(u) - E_m(u)$. The average total mismatch calculated as $[E_p(u) - E_m(u)]/N$ - where N is the number of the considered units - resulted to be 7.9 mm/a and 5.9 mm/a based on suspended/bedload ratios 70/30 and 90/10, respectively. When calculating $E_m(u)$ values by using the average erodibility value $\overline{K}$ as $E_m(u) = \overline{K}\ EI(u)$, the total mismatch increases to 10.4 and 7.7 mm/a, respectively.

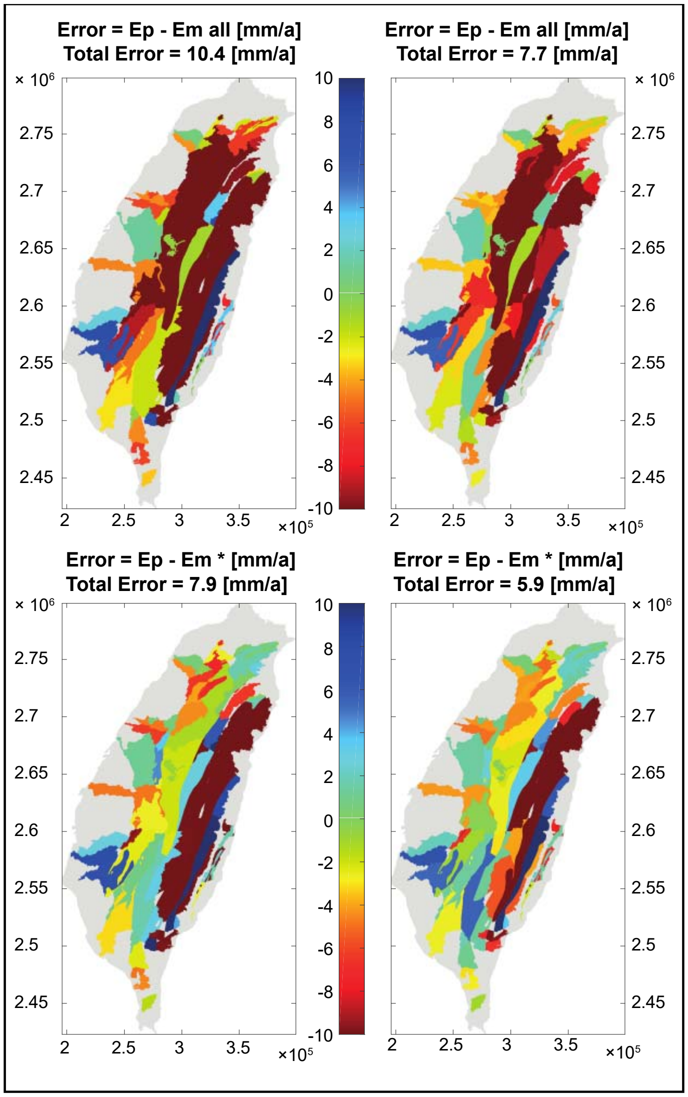

Figure 8: Comparison of provenance-derived and morphometry-derived erosion rates under different assumptions. Top left) suspended/bedload ratio 70/30 and average erodibility value for the entire island. Bottom left) suspended/bedload ratio 70/30 and specific erodibility value for each tectono-stratigraphic unit. Top right) suspended/bedload ratio 90/10 and average erodibility value for the entire island. Bottom right: suspended/bedload ratio 90/10 and specific erodibility value for each tectono-stratigraphic unit. The two techniques agree better when specific erodibility values are considered. Provenance-derived rates are lower in the Backbone Range and Tailuko Belt, whereas morphometry-derived rates are higher in the Yuli Belt downstream.

Although the results obtained by the two applied techniques agree broadly around the island, significant discrepancies are observed particularly on the eastern retro-side of the Central Range. Here provenance-derived rates are notably lower than morphometry-derived rates in the Backbone Range and Tailuko Belt, whereas the opposite is observed in the Yuli Belt downstream (Figure 8). Conversely, on the southwestern pro-side of the orogen provenance-derived rates are higher in the lower tract of the Tsengwen basin, downstream of a major dam. General reasons for discrepancies are diverse, including the heterogeneous distributions of earthquakes, extreme rainfall events and landslides in space and time, and the different timescales investigated by the two techniques.

6.4. The effect of dams

Fluvial sediment fluxes are markedly reduced wherever sediments are trapped in artificial reservoirs upstream of major dams. This effect is particularly drastic for bedload, and may introduce significant bias in our assessment of erosion rates, leading to underestimate the contribution from the units exposed upstream of the dam.

Reservoirs built for agriculture, hydropower and flood management are particularly abundant in the foothill region of western Taiwan. In the Tsengwen catchment, the erosion rates calculated for bedrock units exposed upstream of the Tsengwen and Nanhua reservoirs are much lower than those calculated for units exposed downstream, but similar to those in adjacent mountain catchments, thus suggesting no prominent effect of the dams. In the Zhuoshui catchment, maximum erosion rates are calculated for the Miocene Lushan formation exposed in the headwaters, equally suggesting limited effect of sediment trapping in the Minghu and Mingtan reservoirs. The same lack of major influence by dams is observed in the Dajia catchment.

Despite the major reduction of sediment volumes supplied to the Taiwan Strait owing to the extensive man-made segmentation of sediment-routing systems, sediment composition does not appear to have been altered strongly downstream of the dams, partly owing to reworking of older fluvial deposits, as documented by similar studies in river systems of various sizes from Cyprus, Egypt and China [*Garzanti et al., 2000*; *2015*; *Vezzoli et al., 2016*]. Compositional and/or geochronological signatures of river sediments can thus be used to investigate erosion rates even in strongly anthropized river systems [*Wittmann et al., 2016*].

7. EXHUMATION AND EROSION IN SPACE AND TIME

Apatite and zircon fission-track data document a clear pattern of exhumation across the Taiwan mountains. Long-term erosion rates are generally higher in the axial part of the orogen than in the pro-wedge, and show a general increase from north to south [*Dadson et al., 2003*; *Willet et al., 2003*; *Fuller et al., 2006*]. Erosion patterns on a millennial time scale, as revealed by *in situ* cosmogenic ^{10}Be, show average erosion rates around 4-5 mm/a along the eastern retro-side and of 1-3 mm/a on the western pro-side of the orogen [*Derrieux et al., 2014*]. Erosion rates deduced from cosmogenic ^{10}Be data are usually lower than rates derived from sediment gauging - as documented in the Lanyang catchment [*Siame et al., 2011*] - and closer to rates derived from thermochronometry, although erosion patterns are coherent. This difference may be ascribed to the much shorter timescale investigated by sediment-budget analysis, influenced by stochastic events such as earthquakes or typhoonal downpours.

Extreme rainfall events are common in Taiwan on both sides of the Central Range, acting as an orographic barrier to both easterly typhoons in July-October and the westerly East Asian Monsoon in May-June. Catastrophic earthquakes may occur on both sides of tectonically active Taiwan, with higher frequency along the western pro-side (66 events of magnitude ≥ 6 in the last century, more than one every other year!). During major events, such as the Chi-chi earthquake in 1999 (M_W 7.6; *Shyu et al., 2005*), vertical displacements up to 11 m resulted in the formation of topographic knickpoints [*Huang and Montgomery, 2012*]. Frequency is lower along the eastern retro-side (13 events with magnitude 6.0-6.7 in the last century).

Stream erosion appears to be both transport-limited and supply-limited [*Hovius et al., 2000*]. Earthquakes trigger widespread landslides on the hillslopes, whereas heavy rains allow the evacuation of large amounts of loose detritus made available by landslides. The methods investigating shorter timescales are potentially biased by the complex interplay of such local stochastic events, and do not allow to either support or dismiss the achievement of steady-state conditions, as suggested by previous structural and geomorphic studies of the Taiwan orogen, [*Suppe, 1984*; *Stolar et al., 2007*]. Although erosion rates derived from sediment budgets are typically higher than those inferred from thermochronological data, the spatial pattern is similar [*Dadson et al., 2003*; *Derrieux et al., 2014*], as supported by our provenance-based results.

The study of sediment composition provides indispensable complementary information that allows us to apportion in each catchment the total river load to each single tectono-stratigraphic unit, and thus to calculate the sediment yield from each. In this way we obtain on the one hand a better spatial definition of erosional processes, and on the other hand more robust naturally averaged estimates. Moreover, the method focuses on the entire range of detrital species and can be applied to any set of lithologies and geodynamic settings, overcoming the limitations involved with single-mineral studies (e.g. quartz, apatite, zircon; *Malusà et al., 2015*; *Garzanti, 2016*].

8. CONCLUSIONS

To investigate erosion patterns in the Taiwan orogen we have used petrographic and mineralogical data on modern fluvial sediments, coupled with information from gauged detrital fluxes and insight from the stream-power model. The island of Taiwan is a privileged natural laboratory in which a series of multidisciplinary geomorphological, sedimentological, thermochronological and cosmogenic-nuclide studies have been recently carried out to unravel the impact of geological and climatic processes on rapid mass-wasting in this super-rapidly growing tectonic syntaxis. Our method suffers from various sources of uncertainty, first of which the lack of robustness of sediment-load data and the assumption that sand and mud are derived from the same sources in the same proportions. On the other hand, it allows us to reapportion sediment loads to different lithological units within each catchment, thus leading to a precise identification of tectonic domains undergoing focused erosion.

Our data point to faster erosion of the Backbone Range and Tananao Complex in the central to southern Taiwan, whereas erosion is slower in the northern part of the island undergoing tectonic extension. Although largely based on the same sediment gauging data, the rates we estimate are higher than those inferred by Dadson et al. (2003) because they did not consider the contribution of bedload in their calculations. Our results are consistent with the extreme uplift rates measured with GPS surveys on a decadal timescale, and generally higher than those inferred from cosmogenic-nuclide and thermochronology data reflecting longer timescales. If on the one hand all methods that investigate the complex interplay between tectonic activity, climatic and sedimentary processes are based on various assumptions and suffer from various sources of uncertainty, on the other hand the comparison of results obtained with independent approaches investigating different timescales represents the key to a deeper understanding of the geological and geomorphological evolution of an orogenic belt.

ACKNOWLEDGMENTS

We heartly thank Andrew Tien-Shun Lin, Pei-Hua Hsu and Ming-Wei Liao for fundamental assistance in the field, and Marta Padoan and Giovanni Vezzoli for detailed heavy-mineral and bulk-petrography analyses. Sampling was partially funded by Swiss National Science Foundation Grant Number #200020-131890 to SC. LG acknowledges support from the Israel Science Foundation (grant #707/13). Reviews by ___ and ___ are gratefully acknowledged.

Additional information, including drainage areas, water and solid fluxes, sediment yields and estimated erosion rates from the literature can be found in Appendix Table A1 doi:_____.

Cited references:

1. Aitchison, J. (1986), The statistical analysis of compositional data. Chapman and Hall, London
2. Bonilla, M.G. (1977), Summary of Quaternary faulting and elevation changes in Taiwan. Memoirs of the Geological Society of China, 2, 43-55.

3. Bouchez, J., M. Lupker, J. Gaillardet, C. France-Lanord, and L. Maurice (2011), How important is to integrate riverine suspended sediment chemical composition with depth? Clues from Amazon River depth-profiles, Geochimica et Cosmochimica Acta, 75, 6955-6970.
4. Byrne, T., Y.C. Chan, R.J. Rau, C.Y. Lu, Y.H. Lee, and Y.J. Wang (2011), The Arc-Continent Collision in Taiwan, *in* Arc-Continent Collision edited by D. Brown, and P.D. Ryan, Frontiers in Earth Sciences, pp. 213-246, Springer.
5. Central Geological Survey, Ministry of Economic Affairs (2000), Geological map of Taiwan 1:500000.
6. Chang, S.S.L. and W. R. Chi (1983), Neogene Nannoplankton Biostratigraphy in Taiwan and the Tectonic Implications, Petroleum Geology of Taiwan, 19, 93-147.
7. Ching, K.E., R.J. Rau, K.M. Johnson, J.C. Lee and J.C. Hu (2011), Present-day kinematics of active mountain building in Taiwan from GPS obervations during 1995-2005, Journal of Geophysical Research 116 B09405, doi: 10.1029/2010JB008058.
8. Dadson, S.J., N. Hovius, H. Chen, W.B. Dade, M.L. Hsieh, S.D. Willett, J.C. Hu, M.J. Horng, M.C. Chen, C.P. Stark, D. Lague, and J.C. Lin (2003), Links between erosion, runoff variability and seismicity in the Taiwan orogen, Nature, 426, 648-651.
9. Dadson, S.J., N. Hovius, H. Chen, W.B. Dade, J.C. Lin, M.L. Hsu, C.W. Lin, M.J. Horng, T.C. Chen, J. Milliman, and C.P. Stark (2004), Earthquake-triggered increase in sediment delivery from an active mountain belt, Geology, 32, 733-736.
10. Dadson, S.J., N. Hovius, S. Pegg, W.B. Dade, M.J. Horng, and H. Chen (2005), Hyperpycnal river flows from an active mountain belt, Journl of Geophysical Research: Earth Surface, 110, F04016, doi:10.1029/2004JF000244.
11. Derrieux, F., L.L. Siame, D.L. Vourlès, R.F. Chen, R. Braucher, L. Léanni, J.C. Lee, H.T. Chu, and T.B. Byrne (2014), How fast is the denudation of the Taiwan mountain belt? Perspectives from in situ cosmogenic ^{10}Be, Journal of Asian Earth Sciences, 88, 230-245.
12. Dorsey, R.J. (1988), Provenance evolution and unroofing history in a modern arc-continent collision: evidence from petrography of Plio-Pleistocene sandstones, eastern Taiwan, Journal of Sedimentary Petrology, 58, 208-218.
13. Draper, N.R. and H. Smith (1998), Applied Regression Analysis, 3rd Edition. Wiley.
14. Finlayson, D.P., D.R. Montgomery, and B. Hallet (2002), Spatial coincidence of rapid inferred erosion with young metamorphic massifs in the Himalayas, Geology, 30, 219-222.

15. Fox, M., L. Goren, D.A. May, and S.D. Willet (2014), Inversion of fluvial channels for paleorock uplift rates in Taiwan, Journal of Geophysical Research: Earth Surface, 119, 1853-1875, doi:10/1002/2014JF003196.
16. Fuller, C.W., S.D. Willet, N. Hovius, and R. Slingerland (2003), Erosion rates for Taiwan mountain basins: new determinations from suspended sediment records and a stochastic model of their temporal variation, The Journal of Geology, 111, 71-87.
17. Fuller, C.W., S.D. Willet, D. Fisher, and C.Y. Lu (2006), A thermomechanical wedge model of Taiwan constrained by fission-track thermochronometry, Tectonophysics, 274, 97-115.
18. Garzanti, E. (2016), From static do dynamic provenance analysis – Sedimentary petrology upgraded, Sedimentary Geology, 336, 3-13.
19. Garzanti, E. and S. Andò (2007), Heavy mineral concentration in modern sands: implications for provenance interpretation, *in* Heavy Minerals in use, edited by M.A. Mange and D.T. Wright, Developments in Sedimentology, vol. 58, Elsevier, pp. 517-545.
20. Garzanti, E. and A. Resentini (2016), Provenance control on chemical indices of weathering (Taiwan river sands), Sedimentary Geology, 336, 81-95.
21. Garzanti, E. and G. Vezzoli (2003), A Classification of Metamorphic Grains in Sands Based on Their Composition and Grade, Journal of Sedimentary Research, 73, 830-837.
22. Garzanti, E., S. Andò, and M. Scutellà (2000), Actualistic ophiolite provenance: the Cyprus Case, The Journal of Geology, 108, 199–218.
23. Garzanti E., S. Andò, and G. Vezzoli (2009), Grain-size dependence of sediment composition and environmental bias in provenance studies, Earth and Planetary Science Letters, 277, 422–432.
24. Garzanti, E., S. Andò, M. Padoan, G. Vezzoli, and A. El Kammar (2015), The modern Nile sediment system: Processes and products, Quaternary Science Reviews, 130, 9-56.
25. Glysson, G.D., J.R. Gray, and G.E. Schwarz (2001), A comparison of load estimates using total suspended solids and suspended-sediment concentration data, Proceedings of the 2001 ASCE Water World Congress, Orlando, FL, 20-24.
26. Greensfelder, L. (2002), Subtleties of sand reveal how mountains crumble, Science, 295, 256-258.
27. Hay, W.W. (1998), Detrital sediment fluxes from continents to oceans, Chemical Geology, 145, 287-323.
28. Ho, C.S. (1986), A synthesis of the geologic evolution of Taiwan, Tectonophysics, 125, 1-16.

29. Hovius, N., C.P. Stark, H.T. Chu, and J.C. Lin (2000), Supply and removal of sediment in a landslide-dominated mountain belt; Central Range, Taiwan, The Journal of Geology, 108, 73-89.

30. Huang, M.Y.F. and D.R. Montgomery (2012), Fluvial response to rapid episodic erosion by earthquake and typhoons, Tachia River, central Taiwan, Geomorphology, 175-176, 126-138.

31. Huang, B.S., W.G. Huang, W.T. Liang, R.J. Rau, and N. Hirata, (2006), Anisotropy beneath an active collision orogeny of Taiwan: results from across island array observations, Geophysical Research Letters, 33, L24302, doi: 10.1029/2006GL027844.

32. Hwang, C.-E. (1982), Suspended sediments of Taiwan rivers and their geomorphological significance, Bulletin of National Taiwan Normal University, 27, 649-680.

33. Ingersoll, R.V., A.G. Kretchmer, and P.K. Valles (1993), The effect of sampling scale on actualistic sandstone petrofacies, Sedimentology, 40, 937-953.

34. Jahn, B.M., F. Martineau, J.J. Peucat, and J. Cornichet (1986), Geochronology of the Tananao Schist Complex, Taiwan, and its regional tectonic significance, Tectonophysics, 125, 103-124.

35. Jarvis, A., H.I. Reuter, A. Nelson and E. Guevara (2008), Hole-filled SRTM for the globe Version 4, available from the CGIAR-CSI SRTM 90m Database (http://srtm.csi.cgiar.org).

36. Kao, S.J. and J.D. Milliman (2008), Water and sediment discharge from mountainous rivers, Taiwan: the roles of lithology, episodic events, and human activities, The Journal of Geology, 116, 431-448.

37. Lee, P.J. (1977), Rate of the early Pleistocene uplift in Taiwan, Geological Society of China Memoirs, 2, 71-76.

38. Li, Y.H. (1976), Denudation of Taiwan Island since the Pleistocene epoch, Geology, 4, 105-107.

39. Lin, A.T., A.B. Watts, and S.P. Hesselbo (2003), Cenozoic Stratigraphy and Subsidence History of the South China Sea Margin in the Taiwan Region, Basin Research, 15, 453-478.

40. Liu, T.K. (1982), Tectonic implication of fission track ages from the Central Range, Taiwan, Proceedings of the Geological Society of China, 25, 22-37.

41. Liu, C.-C. and S.-B. Yu (1990), vertical crustal movements in eastern Taiwan and their tectonic implications, Tectonophysics, 183, 111-119.

42. Liu, J.P., C.S. Liu, K.H. Xu, J.D. Milliman, J.K. Chiu, S.J. Kao, and S.W. Lin (2008), Flux and fate of small mountainous rivers derives sediments into the Taiwan Strait, Marine Geology, 256, 65-76.

43. Lundberg, N. and R.J. Dorsey (1990), Rapid Quaternary emergence, uplift, and denudation of the Coastal Range, eastern Taiwan, Geology, 18, 636-641.
44. Lupker, M., C. France-Lanord, J. Lavé, J. Bouchez, V. Galy, F. Métivier, J. Gaillardet, B. Lartiges, and J.-L. Mugnier (2011), A Rouse-based method to integrate the chemical composition of river sediments: Application to the Ganga basin, Journal Of Geophysical Research, 116, F04012, doi: 10/1029/2010JF001947.
45. Maddock, T., and W.M. Borland (1950), Sedimentation Studies for the Planning of Reservoirs by the Bureau of Reclamation. Technical Report, United States Department of the Interior, Bureau of Reclamation, Hydrology Division.
46. Malavieille, J., S.E. Lallemand, S. Dominguez, A. Deschamps, C.Y. Lu, C.S. Liu, and P. Schürnle (2002), Arc-continent collision in Taiwan: New marine observations and tectonic evolution. *in* Geology and Geophysics of Arc-Continent collision, Taiwan, Republic of China edited by T.B. Byrne, and C.S Liu, Geological Society of America Special Paper 358, 189-213.
47. Malusà, M.G., A. Resentini, and E. Garzanti (2016), Hydraulic sorting and mineral fertility bias in detrital geochronology, Gondwana Research, 31, 1-19.
48. Martin-Fernandez, J.A., C. Barcelo-Vidal, and V. Pawlowsky-Glahn (2003), Dealing with zeros and missing values in compositional data sets using nonparametric imputation, Mathematical Geology, 35 (3), 253-278.
49. McIntosh, K., H. van Avendonk, L. Lavier, W.R. Lester, D. Eakin, F. Wu, C.S. Liu, and C.S. Lee (2013), Inversion of a hyper-extended rifted margin in the southern Central Range of Taiwan, Geology, 41, 871-874.
50. Montgomery, D.R., M.Y.F. Huang, and A.Y.L. Huang (2014), Regional soil erosion in response to land use and increased typhoon frequency and intensity, Taiwan, Quaternary Research, 81, 15-20.
51. Mouthereau, F., B. Deffontaines, O. Lacombe, and J. Angelier (2002), Variations Along the Strike of the Taiwan Thrust Belt: Basement Control on Structural Style, Wedge Geometry, and Kinematics, *in* Geology and Geophysics of Arc-Continent collision, Taiwan, Republic of China edited by T.B. Byrne, and C.S. Liu, Geological Society of America Special Paper 358, 31-54.
52. Nagel, S., S. Castelltort, E. Garzanti, A.T. Lin, S.D. Willett, F. Mouthereau, M. Limonta, and T. Adatte (2014), Provenance evolution during arc-continent collision: sedimentary petrography of Miocene to Pleistocene sediments in the western foreland basin of Taiwan, Journal of Sedimentary Research, 84, 513-528.

53. Peng, T.H., Y.H. Li, and F.T. Wu (1977), Tectonic uplift rates of the Taiwan Island since the Early Holocene, Memoirs of the Geological Society of China, 2, 57-69.

54. Porterfield, G. (1972), Computation of fluvial-sediment discharge, US Government Printing Office.

55. Pratt-Sitaula, B.A., M. Garde, D.W. Burbank, M. Oskin, A. Heimsath, and E.J. Gabet (2007), Bedload-to-suspended load ratio and rapid bedrock incision from Himalayan landslide-dam lake record, Quaternary Research, 68, 111–120.

56. Schaller, M., N. Hovius, S.D. Willet, S. Ivy-Ochs, H.A. Synal, and M.C. Chen (2005), Fluvial bedrock incision in the active mountain belt of Taiwan from in situ-produced cosmogenic nuclides, Earth Surface Processes and Landforms, 30, 955-971.

57. Shellnut, J.G., A. Belousov, M. Belousova, K.L. Wang, and G.F. Zellmer (2014), Generation of calc-alkaline andesite of the Tatun volcanic group (Taiwan) within an extensional environment by crystal fractionation, International Geology Review, 56, 1156-1171.

58. Shinjio, R., S.L. Chung, Y. Kato, and M. Kimura (1999), Geochemical and Sr-Nd isotopic characteristics of volcanic rocks from the Okinawa Trough and Ryukyu Arc: implications for the evolution of a young, intracontinental back arc basin, Journal of Geophysical Research, 104, 10591-10608, doi:10.1029/1999JB900040.

59. Shyu, J.B.H., K. Sieh, Y.G. Chen, and C.S. Liu (2005), Neotectonic architecture of Taiwan and its implications for future large earthquakes, Journal of Geophysical Research, 110, B08402, doi: 10.1029/2004JB003251.

60. Siame, L.L., J. Angelier, R.F. Chen, V. Godard, F. Derrieux, D.L. Bourlès, R. Braucher, K.J. Chang, H.T. Chu, and J.C. Lee (2011), Erosion rates in an active orogen (NE-Taiwan): a confrontation of cosmogenic measurements with river suspended loads, Quaternary geochronology, 6, 246-260.

61. Simoes, M., J.P. Avouac, O. Beyssac, B. Goffé, K.A. Farley and Y.G. Chen (2007), Mountian building in Taiwan: a thermokinematic model, Journal of geophysical research, 112, B11405, doi: 10.1029/2006jb004824.

62. Simoes, M., O. Beyssac, and Y.G. Chen (2012), Late Cenozoic metamorphism and mountain building in Taian: a review, Journal of Asian Earth Sciences, 46, 92-119.

63. Sklar, L.S. and W.E. Dietrich (2001), Sediment and rock strength controls on river incision into bedrock, Geology, 29, 1087-1090.

64. Song, R.S., T.F. Yanf, Y.H. Yeh, S. Tsao, and H.C. Lo (2000), The Tatun Volcano Group is active or extinct?, Journal of the Geological Society of China, 43, 521-534.

65. Stolar, D.B., S.D. Willet, and D.R. Montgomery (2007), Characterization of the topographic steady state in Taiwan, Earth and Planetary Science Letters, 261, 421-433.
66. Suppe, J. (1984), Kinematics of arc-continent collision, flipping of subduction, and the back-arc spreading near Taiwan, Memoir of the Geological Society of China, 6, 21-33.
67. Teng, L.S. (1996), Extensional collapse of the northern Taiwan mountain belt, Geology, 24, 949-952.
68. Teng, L.S., Y. Wang, C.H. Tang, T.C. Huang, M.S. Yu, and A. Ke (1991), Tectonic aspects of the Paleogene depositinal basin of Northern Taiwan, Proceedings of the Geological Society of China, 34, 313-336.
69. Turowski, J.M., D. Rickenmann, and S.J. Dadson (2010), The partitioning of the total sediment load of a river into suspended load and bedload: a review of empirical data, Sedimentology, 57, 1126-1146.
70. Vermeesch, P., A. Resentini, and E. Garzanti (2016), An R package for statistical provenance analysis, Sedimentary Geology, 336, 14-25.
71. Vezzoli, G., E. Garzanti, M. Limonta, S. Andò, and S. Yang (2016), Erosion patterns in the Changjiang (Yangtze River) catchment revealed by bulk-sample versus single-mineral provenance budgets, Geomorphology, 271, 177-192.
72. Wang, K.L., S.L. Chung, S.Z. O'Reilly, S.S. Sun, R. Shinjo, and C.H. Chen (2004), Geochemical constraints for the genesis of post-collisional magmatism and the geodynamic evolution of the northern Taiwan region, Journal of Petrology, 45, 975-1011.
73. Weltje, G.J. (1997), End-member modeling of compositional data: numerical-statistical algorithms for solving the explicit mixing problem, Mathematical Geology, 29, 503-549.
74. Whipple, K.X., and G.E. Tucker (1999), Dynamics of the stream-power river incision model: implications for height limits of mountain ranges, landscape response timescales, and research needs, Journal of Geophysical Research, 104, 17661-17674, doi:10.1029/1999JB900120.
75. Willett, S.D., D. Fisher, C. Fuller, Y. En-Chao, and L. Chia-Yu (2003), Erosion Rates and Orogenic-Wedge Kinematics in Taiwan Inferred from Fission-Track Thermochronometry, Geology, 31, 945-948.
76. Wittmann, H., M.G. Malusà, A. Resentini, A., E. Garzanti, and S. Niedermann (2016), The cosmogenic record of mountain erosion transmitted across a foreland basin: source-to-sink analysis of in situ ^{10}Be, ^{26}Al and ^{21}Ne in sediment of the Po river catchment, Earth and Planetary Sciences Letters, *in review*.

77. Wobus, C., K.X. Whipple, E. Kirby, N. Snyder, J. Johnson, K. Spyropolou, B. Crosby, and D. Sheehan (2006), Tectonics from topography: Procedures, promise, and pitfalls, Geological Society of America Special Papers, 398, 55-74.